Transp Porous Med (2017) 117:169–187
DOI 10.1007/s11242-017-0827-y

Consideration on Data Dispersion for Two-Phase Flow Micromodel Experiments

S. Marchand[1,2] · I. Bondino[1] · A. Ktari[1,3] · E. Santanach-Carreras[4,5]

Received: 24 May 2016 / Accepted: 24 January 2017 / Published online: 27 February 2017

Abstract Transparent man-made porous media, also known as micromodels, are a widely used exploration tool in the field of two-phase flow in porous media (Alireza and Sohrabi in Soc Petrol Eng 166435, 2013; Bondino et al., in International symposium of the society of core analysts held in Napa Valley, California, USA, 2013) to enhance the comprehension of oil recovery mechanisms at pore-scale. Although they have more often been used as qualitative visualization tools to explore the elementary physicochemical features of a given flow mechanism, their utilization as a quantitative tool is interesting especially in industrial context, where they represent an easy and low-cost screening tool for complex recovery mechanisms (low salinity waterflooding, polymer flooding, etc). However, the repeatability of these experiments and thus the possibility to derive quantitative conclusions from them appears not to be investigated in the literature in our field of study. In this work, we explore the dispersion of data such as capillary desaturation curves and secondary waterflood recoveries using micromodels of different sizes and different pore patterns from our laboratory and from an external one. Using datasets with low sampling (low number of repeats of an experiment) and with very large sampling, we document the type of data dispersion, we analyze its

✉ S. Marchand
soph.march@gmail.com

I. Bondino
igor.bondino@total.com

A. Ktari
ktari.amir91@gmail.com

E. Santanach-Carreras
enric.santanach-carreras@total.com

1 Total S.A., CSTJF, Avenue Larribau, 64018 Pau, France

2 Present Address: ESPCI Paris, 10 Rue Vauquelin, 75005 Paris, France

3 Present Address: Technica Engineering GMBH, Leopoldstrasse 236, 80807 Munich, Germany

4 Total S.A., Pôle d'Etudes et Recherche de Lacq, BP 47 64170, Lacq, France

5 Laboratoire Physico-Chimie des Interfaces Complexes, Total S.A. - ESPCI, RD 817, 64170 Lacq, France

reasons and we verify to which extent truly quantitative conclusions can be drawn from these datasets. Our study demonstrates that at low sampling drawing quantitative inferences from our datasets is questionable due to the large uncertainty of the produced data.

Keywords Repeatability · Pore-scale · Sampling

1 Introduction

For thirty years, micromodels have shown to be valuable tools for the study of two-phase flow displacement processes (Karadimitriou and Hassanizadeh 2011). The improvement on techniques of micromodel manufacturing is still continuing in particular to monitor the pore pattern geometry (Karadimitriou et al. 2012) as well as to improve the representation of the rock environment (Porter et al. 2015; Song and Kovscek 2015; Sohrabi et al. 2015; Schneider 2011). Among the recent advances in visualization, confocal microscopy techniques have been used to explore the behaviors of two-phase flow through three-dimensional porous medium (Datta et al. 2014a). Several researchers have studied these displacement processes with the aim of improving their understanding by evaluating the influence of parameters such as wettability (Cottin et al. 2011), by exploring specific phenomena such as Haines jumps (Armstrong and Berg 2013), by examining the transition between imbibition regimes (Levaché 2014) or by observing the dynamics of ganglia population in the porous medium (Datta et al. 2014b). Data obtained from micromodel experiments are used to validate simulators for numerous processes: drainage (Cottin et al. 2010), viscous fingering patterns (Doorwar and Mohanty 2014) or Haines jumps'scales (Armstrong et al. 2015). Indeed, those micromodel results are displayed in the form of the following variables: porosity, permeability, fluid desaturation patterns and recovery factors which are accessible by micromodel visualization (Buchgraber et al. 2012) and are widely used for Enhanced Oil Recovery (EOR) studies. Among them, research works were performed on low salinity waterflooding (Bondino et al. 2013; Emadi et al. 2012) or on polymer use (Sedaghat et al. 2013; AlDousary 2012; Buchgraber et al. 2011).

In some of the micromodel utilizations reported above, quantitative information on oil recovery performance was reported, for example, about the effect of different polymer solutions (Sedaghat et al. 2013). This quantitative use is particularly important as it can allow rapid screening of flow protocols in microfluidics devices. Nevertheless, issues of repeatability and/or statistical relevance are generally not discussed (at least in an explicit format) or properly documented in the literature as it should be when trying to derive quantitative information. It is therefore the objective of this work to estimate oil recovery data dispersion for two typical micromodel datasets: In this work, we estimate this variability in detail for the important case of the capillary desaturation curve (CDC) (Rodriguez de Castro et al. 2015). Using four different pore patterns, we replicate the measurement of CDC in order to illustrate the associated data dispersion. For the same objective, our focus then shifts to waterflood recoveries with a fifth pore pattern associated with a larger dataset of 58 experimental replications. Although the specific variability in the two datasets available in this study cannot be generalized to other datasets or other Laboratories, our results and associated analysis help elucidate the observed data dispersion by means of statistical tools and provide insight on the possible utilization of the micromodel tool for derivation of quantitative information.

2 Material and Methods

2.1 Dataset 1

Dataset 1 was acquired to study capillary desaturation in water wet conditions and its possible relation with pore pattern. The experimental setup is composed of a porous medium connected to a microfluidic circuit. The porous medium is made of two B270 glass layers bonded together at high temperature (Dolomite, Royston, UK). Once a pore pattern is drawn using a CAD software, the 2D chip is obtained by etching the glass with HF acid: This etching can be done on both glass layers (double etching) or on only one glass layer (single etching). In the first case, the two glass plates are bonded in order to have superposition of the pore patterns (misalignment between the two etched surfaces can be up to +/−5μm). Without specific treatment, this system is transparent and hydrophilic. In our study, four micromodel types (MT) are used, with characteristics given in Table 1. Micromodel have pore pattern dimension of 60.00 × 60.69 mm (with a tolerance of ±0.1 mm) with a constant etch depth; external overall physical dimensions of the chip are 65 × 90 × 4 mm (with a tolerance of ±0.1 mm). Concerning the micromodel, type 4 has a pore pattern of 58.94 × 59.65 mm (with a tolerance of ±0.1 mm). Note that each channel in the micromodel, type 2 holds a constriction (see Fig. 2a): Constrictions are of two types, the first with depth and width of 14 ± 4.5 μm and 14 ± 5.0 μm, respectively, and the second with 14 ± 4.5 and 25 ± 5.0 μm: such constrictions are visible in the form of pore throats in Fig. 1.

In order to provide an estimate for the pore volumes of our four different pore patterns, a combination of experimental image analysis were used. First the pore patterns are 100% saturated with a dye solution (methylene blue): The number of pixels corresponding to the colored phase in the pore pattern is counted. In a second experiment, the non-wetting phase used in our experiments is injected until breakthrough and the relation between pixels of the non-wetting phase and volume injected is noted down. This linear relation is then used to find the volume injected that corresponds to the pixel count for the 100% saturated pore pattern. Concerning the porosity, it is defined as the ratio of this pore volume on the pore pattern volume where the cross section is defined as the product of the channel depth by the pore pattern width. The associated uncertainty is determined by Eq. 1 (JCGM 2008; Taylor 2000).

$$\frac{\delta A}{A} = \sqrt{\left(\frac{\delta l}{l}\right)^2 + \left(\frac{\delta d}{d}\right)^2} \tag{1}$$

where A is the cross section, l is the width of the pore pattern and d is its depth. The channel depth uncertainty is given by manufacturer's information and the uncertainty associated with the mask width is estimated as negligible compared to the one of the effective channel width etched (±2 μm from manufacturer's details).

According to the manufacturer information, the surface roughness of the inside channel is $R_a \approx 5$ nm, with R_a the arithmetic average of the roughness profiles. Note that due to wet etching technique (Karadimitriou et al. 2012), the channel width is set by the mask width and the channel depth (Fig. 2).

Concerning the microfluidic circuit, we use plastic tubing of outer diameter of 0.25mm in ethylene-tetrafluoroethylene (CIL, Sainte-Foy-La-Grande, France, Model: 1529L) with conical connectors (CIL, Sainte-Foy-La-Grande, France, Model: LT-110x, LT-110x); and switching valves (CIL, Sainte-Foy-La-Grande, France, Model: V-101L, p-732). Flow rates are applied to the porous medium with a syringe pump (Fisher Scientific, Strasbourg, France,

Table 1 Summary of properties of the micromodel types (MT) used for the dataset 1

Micromodel type	Etching technique	Channel depth (μm)	Mask channel width (μm)	Pore volume (μL)	Porosity (%)	Cross section (mm^2)
MT1	Single etching	50 ± 2	10–150	≈ 120	≈ 55.4	3.000 ± 0.005
MT2	Double etching	30 ± 2	35–80	≈ 82	≈ 56.0	1.800 ± 0.003
MT3	Double etching	50 ± 2	10–68	≈ 52	≈ 29.0	3.000 ± 0.005
MT4	Single etching	150 ± 2	30–300	≈ 320	≈ 59.0	8.80 ± 0.01

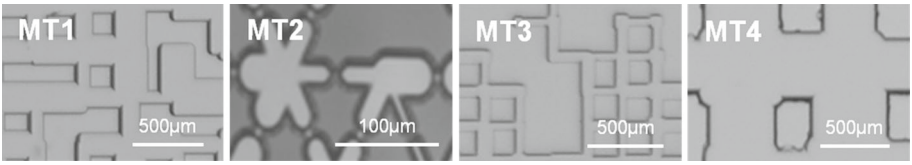

Fig. 1 Details of the pore patters for each micromodel type (MT)

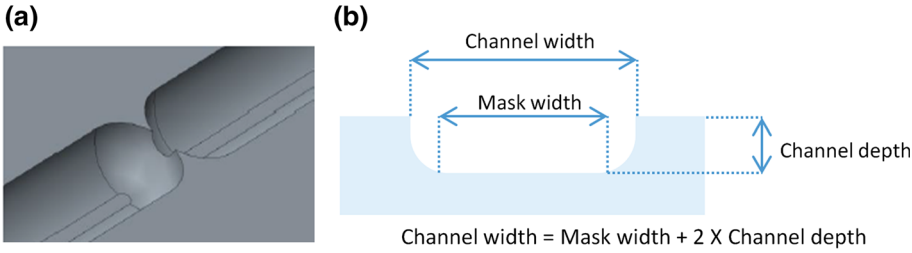

Fig. 2 **a** Schematic detail for a pore constriction for MT2, **b** Generic representation of the relationship between channel geometry parameters for wet etching

Model: 789100I). To inject the fluids, we use syringes of 1 mL (CIL, Sainte-Foy-La-Grande, France, Model: 4001TLL) or 10 mL (Fisher Scientific Strasbourg, France, Model: 10098330).

2.1.1 Protocol

All the experiments are performed under laboratory pressure and at room temperature. For a given micromodel type (MT), repeats are conducted using any of two identical samples provided by the manufacturer: In other words a set of three repetition experiments is conducted on two samples that differ by only the construction tolerance. This optimizes experimental time as there is always one sample available, while the other is being subjected to cleaning. Each experiment consists of the following steps (see also Figs. 3, 4).

(1) The pore pattern in the micromodel is cleaned with three successive injections of 1 mL of toluene then acetone repeated at each entry of the device. After oven-drying at 60 °C (around 20 min), the pore pattern is similarly washed with a solution of Nochromix® (Sigma-Aldrich, Missouri, USA, Product: 328693 Aldrich) at 23 g L^{-1} in sulfuric acid 25%. Each of the above-mentioned injections is repeated after a rest interval of 5 min. Then, the following injection steps are operated: injection of distilled water, followed by injection of a basic solution of potassium chloride (KCl) at 30 g L^{-1} in distilled water, again distilled water followed by acetone. To finish, the micromodel is dried in an oven at 60 °C. The injections above are operated on a cleaning rig apparatus, separate from the experimental rig detailed below. A brand-new sample is not subjected to the cleaning procedure above, but only flushed with acetone and distilled water, directly on the experimental rig.
(2) The micromodel is fixed on its in-house chip holder, designed in order to limit the entry/exit dead volumes to approximately 5 µL. Before the chip holder is mounted on the rig, the tubing circuit is cleaned manually with an injection of toluene followed by acetone.
(3) At this point, with the micromodel in place on the rig and in vertical position (see Fig. 3), acetone is injected in the microfluidic system to saturate the now-mounted micromodel.

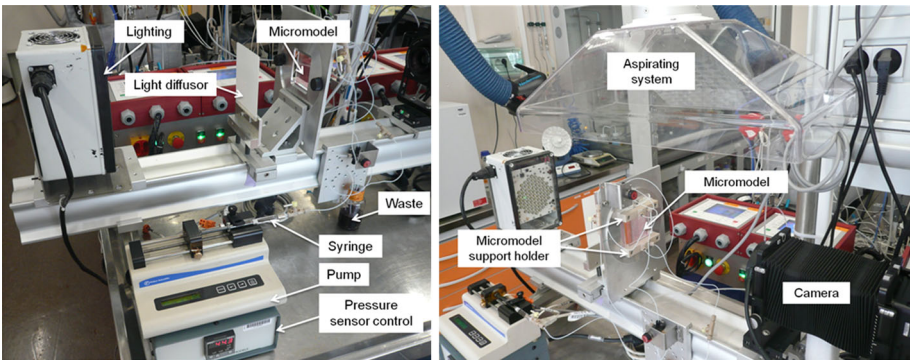

Fig. 3 Photographs of the rig

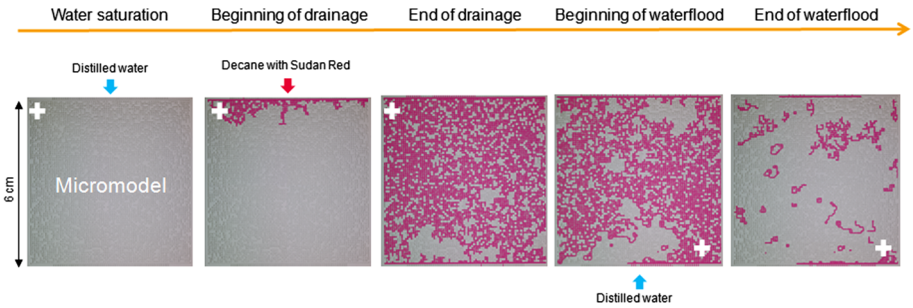

Fig. 4 Schema of the principal experimental steps

Then, all system is dried with nitrogen and vacuumed. To finish, distilled filtered water is manually injected in order to saturate the micromodel. The unwanted presence of air bubbles is checked in a high-resolution photograph of the pore patterns: If air bubbles are found, then the whole step (3) is repeated.

(4) At the top of the saturated micromodel, the non-wetting phase, a solution of Sudan Red 7B (Sigma-Aldrich, Missouri, USA, Product: 53373 Sigma-Aldrich) in *n* decane of $\approx$ 100 g L^{-1} is injected at 80 µL/h, in order to drain the pore pattern. Once the distribution of this colored phase in the micromodel is visually stable, the drainage is estimated as completed. The interfacial tension between distilled water and decane was measured at 23.74 $\pm$ 0.01 mN m^{-1}.

(5) The micromodel is turned upside down on the rig, and the waterflood is performed from the bottom with distilled water. In this way, we make sure both oil and water injections use the same inlet, and at the same time, we maintain gravity stable conditions. The desaturation is performed by passing distilled water through the micromodel device at increasing and incremental flow rates (taken between 20 µL/h and 127 mL/h). Before moving to a successive higher water flow rate, visual checks are made on our live screen that the system is stable.

2.1.2 Image Acquisition and Processing

Various 2D images were taken for each incremented flow rate. The acquisition frame is set to obtain at least four images for a given flow rate state. The image acquisition is performed

with a camera (Phase One, Copenhagen, Denmark, Product: IQ180 Camera System) linked to a computer in order to display the images by the Capture One 7 software (Phase One, Copenhagen, Denmark). The porous medium is lightened by a set of LEDs (CREE, North Carolina, USA, Model: XLamp XP-E LED). The image resolution and position stay identical during an experiment and are, respectively, 7760 × 10,328 pixels and centered on the middle of the porous medium. Thus, a complete image of the micromodel is obtained and is then cropped in order to isolate the porous medium. A fully developed TIFF image has a size of approximately 230 Mb. For each flow rate state, only the last acquired image is analyzed with ImageJ, a public domain image processing program, in order to extract information about the distribution of organic phase in the porous medium. The image analysis consists first in the cropping and in the segmentation of the porous medium area. The segmentation is performed in order to extract the colored phase from the image. Then, the "analyze particles" tool is used to obtain information about the distribution of this colored phase. This information is arranged in Microsoft® Excel 2007 documents from which the graphs of this study are created.

2.1.3 Errors and Limits Associated with the Experimental and Processing Procedure

In this paper, we define saturation of a phase in terms of the 2D visible pore occupancy from a pixel count in a photograph. This means that we do not attempt to reconstruct the 3D saturation as the pore geometries, shapes and cross sections vary in the third dimension from one pore pattern to the other. Furthermore, we do not have access to the pore filling state in the third dimension. These factors represent a limitation in the conclusions we can derive from this work.

Concerning the experimental instruments, we use a syringe pump to control the value of the flow rate applied, and according to manufacturer's instructions, the error on the flow rate value is of 1%. Then, the quality of the image capture process depends on the resolution limit of the video camera with respect to the size of the features of interest. Finally, as we extract our data from the segmented pixels, errors can come from the cropping (not necessarily identically repeated from one photograph to the next), the segmentation of the images and the lighting of the micromodel (which can be subject to subtle variations during the course of the day).

Knowing the dimensions of the porous medium, with ImageJ, we measure the corresponding number of pixels on a sample of four experimental images. By averaging on three measures, we obtain a resolution limit of $8\,\mu\mathrm{m\,px}^{-1}$.

The cropping error is evaluated by carrying out the image analysis on photographs from different experiments in order to have different tilts of the image. Moreover, to have a complete view of this error, we take for each experiment one image at the beginning of flow rate application and the other at the end of it. We do three times the cropping on the same images and extract the variables of interest. For a given variable and a given image, we calculate the ratio between the standard deviation and the average. Then, considering all the analyzed images, we choose to take the rounded average of these ratios as the estimation of the cropping error. Thus, we have an estimated error of 4 and 3%, respectively, for the number of blobs and the total area of pixels corresponding to the area covered by the decane phase.

Regarding the segmentation of the images, we carry out a study with pore pattern MT1 for each of its three experiments and for four flow rates (300, 2000, 100,000 and 126,900 μL/h). To modify the segmentation, we change the lowest limit of hue (HSB-RGB color model), with the "Threshold" tool of ImageJ, keeping the upper limit to 255. From this study, we

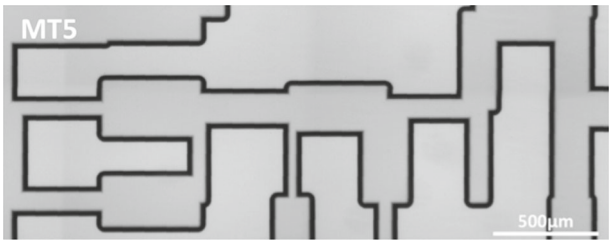

Fig. 5 Details of the pore patters for micromodel type used for the dataset 2

can estimate that the error from the segmentation is negligible (one order of magnitude of difference) compared to the one coming from cropping for the number of blobs and the total area of pixels. Note that for all the precedent image analysis work, we keep the lowest limit of hue between 192 and 227 (we choose 192, 224 and 227). To extend this conclusion to the other micromodel types, we considered the repartition of the peaks in HSB model finding similar repartition in the HSB-RGB color peaks (see Fig. 5).

2.1.4 Dataset 1 Content and Nomenclature

We dispose of a dataset of high-resolution images of 13 micromodel experiments on 4 pore patterns (that is, experiments are repeated 3 or 4 times on a given pore pattern). Image analysis is used to segment the pixels of the organic phase (which will be referred as the oil phase) and of the aqueous phase. Thus, we have 2D global information about oil distribution in terms of applied flow rate. This dataset can be organized as follows. We consider the variables i, j, q which, respectively, represent the micromodel type, the number of the experiment (for a given micromodel type) and the flow rate applied in µL/h. Note that for a given flow rate stage, we consider only one image in our analysis, the one at the end of the flow rate application; for a given experiment, approximately thirty flow rate increments are applied. Then, an image corresponding to a given state of an experiment is referred to as MTi_EXPj_q. For example, the image obtained with the micromodel type 2, in the third experiment and at the end of the flow rate period equal to 1000 µL/h is referred as MT2_EXP3_1000. Note that the dataset we consider is such as $i = \{1, 2, 3, 4\}$; $j_{i\neq 4} = \{1, 2, 3\}$, $j_{i=4} = \{1, 2, 3, 4\}$; $q = [0, 126900]$ with $q = 0$ referring to the initial state (before any flow rate is applied). For MT4_EXP4, we have fewer values for q than for the other MT4 experiments due to a pump failure that led us to stop the experiment: For this reason, the experiment MT4_EXP4 is not used in our statistical analysis because our statistical statement will be made for all MT at the same number of replications. However, MT4_EXP4 is plotted in Fig. 6 as an argument for the general behavior of the dataset MT4.

2.2 Dataset 2

Dataset 2 is part of an historical experimental database targeting tertiary EOR (enhanced oil recovery) that could be available for study to the authors. Although the tertiary EOR experiments explored a number of different injection protocols and mechanisms, the secondary waterfloods are all repetitions in identical conditions. We note that that the experiments and the image processing were not performed by the authors: The authors are simply using an available dataset from another laboratory to support and demonstrate some statistical conclusions regarding dataset 1. This dataset is presented here in a concise manner. Similarly to

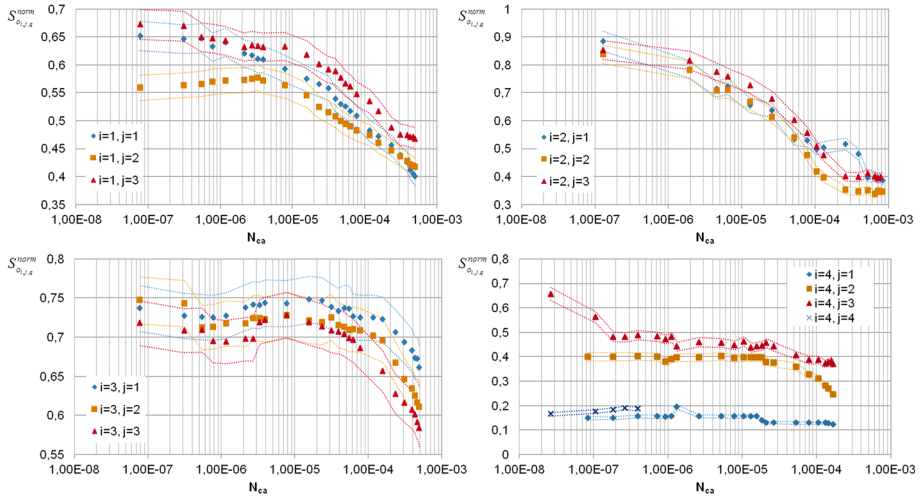

Fig. 6 $S_{o_{i,j,q}}^{\text{norm}}$ in terms of N_{ca} for each micromodel type (*solid markers*); *dashed lines* define the uncertainty (b-type) interval associated with each experiment

Table 2 Summary of properties of the micromodel type used for the dataset 2

Micromodel type	Etching technique	Channel depth (μm)	Mask channel width (μm)	Pore volume (μL)	Porosity (%)	Cross section (mm^2)
MT5	Single etching	≈ 40	112–337	≈ 15.4	≈ 53.0	≈ 0.5

the experimental setup presented above, dataset 2 is also composed of a glass micromodel connected to a microfluidic circuit. The external overall physical dimensions of this micromodel are: 62.5 × 12.5 × 2.2 mm and the pore pattern dimension is of 62.5 × 12.5 mm with a constant etch depth. More information about the micromodel's properties is given in Table 2, while Fig. 5 illustrates the pore pattern arrangement. The micromodel is kept filled with distilled water. At the first experimental step, the water initially contained in the micromodel is chased away by carbon dioxide. Then, brine is used to saturate the micromodel, and finally, a drainage step is performed at 1 μL/min with crude oil of viscosity 2000 cp (extra-heavy oil). The dataset gathers 58 replications of the waterflood experiment that consists in injecting three pore volume of brine (see Table 3 for composition) into the oil-saturated micromodel at 0.2 μL/min. After each experiment, the glass micromodel was cleaned with the same procedure of dataset 1 to restore the hydrophilic nature of the material; occasionally, a micromodel would become unusable and would be substituted by an identical replica. All experiments were done at room conditions of temperature and pressure. Images of the micromodel are taken every 10 s, and percentages of oil recovery are obtained by image processing. Note that the dataset we consider is such that sss j represent the number of the experiment with $j = [1, 58]$ as the micromodel type and the flow rate are fixed for each experiment. It is worthy noticing that this dataset was achieved by different human operators, using a different experimental rig in a different geographical location and approximately 3 years before the construction of dataset 1.

Table 3 Description of the brine composition, final concentration of the salts (dissolved in distilled water)

Salt type	$NaHCO_3$	KCl	NaCl
Concentration (g/L)	3.47	0.13	4.19

3 Oil Saturation Study

In petroleum field, for microscopic scale experiments, oil saturation is the usual variable of interest (Chatzis et al. 1983; Jadhunandan and Morrow 1995; Iglauer et al. 2012) and thus, to compare our results with the literature, this variable is selected to perform the first part of the study. We note this variable as $S^{\text{norm}}_{o_{i,j,q}}$, its definition given by Eq. 2.

$$S^{\text{norm}}_{o_{i,j,q}} = \frac{S_{o_{i,j,q}}}{S_{o_{i,j,0}}} \tag{2}$$

where the normalization is done with respect to the oil saturation $S_{o_{i,j,0}}$ at the beginning of the experiment (end of drainage phase). As we have several experiments (labeled by the variable j) for each micromodel type and at a given flow rate (or capillary number), we can define the average of the oil saturation as follows (Eq. 3).

$$\overline{S^{\text{norm}}_{o_{i,q}}} = \frac{\sum_{j=1}^{n} \frac{S_{o_{i,j,q}}}{S_{o_{i,j,0}}}}{n} \tag{3}$$

where n is the number of experiment repetitions performed. $S^{\text{norm}}_{o_{i,j,q}}$ data are plotted in terms of capillary number (Chatzis and Morrow 1984) N_{ca} (Eq. 4).

$$N_{ca} = \frac{v \times \mu}{\sigma} \tag{4}$$

$$v = \frac{q}{A} \tag{5}$$

with v the Darcy velocity (Eq. 5), μ the viscosity of the displacing phase, σ the interfacial tension between the two considered phases, q the applied flow rate and A the cross section of the micromodel (reported in Table 1). Each graph in Fig. 6 represents the replication experiments performed for a given micromodel type.

The plotted uncertainties, drawn by the dashed lines and derived from Eq. 6, represent the uncertainty interval associated with b-type uncertainty coming from image processing (see paragraph "Errors and limits associated with the experimental and processing procedure"). There is no a-type uncertainty as we consider the experiment individually (this terminology comes from JCGM (2008): An a-type uncertainty arises from the statistical analysis of a dataset for a fixed variable type; a b-type uncertainty refers to all the uncertainties coming from other methods than the statistical one (e.g., manufacturer's information)).

$$\frac{\delta S^{\text{norm}}_{o_{i,j,q}}}{S^{\text{norm}}_{o_{i,j,q}}} = \sqrt{\left(\frac{\delta S_{o_{i,j,q}}}{S_{o_{i,j,q}}}\right)^2 + \left(\frac{\delta S_{o_{i,j,0}}}{S_{o_{i,j,0}}}\right)^2} \tag{6}$$

As $\frac{\delta S_{o_{i,j,q}}}{S_{o_{i,j,q}}} = \frac{\delta S_{o_{i,j,0}}}{S_{o_{i,j,0}}} = 0.03$ (see Material and methods), then $\frac{\delta S^{\text{norm}}_{o_{i,j,q}}}{S^{\text{norm}}_{o_{i,j,q}}} = 0.04$. Concerning the uncertainty in the derivation of N_{ca}, we use Eq. 7 derived from Eq. 4.

$$\frac{\delta N_{ca}}{N_{ca}} = \sqrt{\left(\frac{\delta q}{q}\right)^2 + \left(\frac{\delta \mu}{\mu}\right)^2 + \left(\frac{\delta \sigma}{\sigma}\right)^2 + \left(\frac{\delta A}{A}\right)^2} \tag{7}$$

By calculation, we find that for all micromodel types, we have $\frac{\delta N_{ca}}{N_{ca}} = 0.01$. As this uncertainty is small and constant regardless of micromodel type, it is not represented in Fig. 6, also to make the information in the graphs more legible.

In Fig. 6, we can note that, for all the experiments, the initial value of oil saturation corresponding to $N_{ca} = 0.$ (the notation for the stage right after drainage) has not been represented as its value is constant (equal to 1 due to normalization choice) and that we choose a logarithmic x axis. For all the micromodel types, $S^{\text{norm}}_{o_{i,j,q}}$ tends to decrease when the flow rate corresponding to the experimental state is increasing; the identification of a critical capillary number signaling the onset of desaturation is in general not trivial. We note an imprint of the pore pattern in that for MT2 very little oil was produced after the first waterflood, with desaturation being then very effective ($\Delta S^{\text{norm}}_{o_{i=2,j,q}}$ is around 40%). For MT3 on the other hand, desaturation is the least effective, a conclusion that can be extended to MT4 as well although this case is quite heterogeneous (see discussion below).

Considering each micromodel type individually, in order to highlight specific trends, for MT1 we observe that the experiments corresponding to MT1_EXP1 and MT1_EXP3 have a similar curve's shape and values than the ones of MT1_EXP2 and that their intervals of confidence intersect for every N_{ca}. The offset observed between the curves of a same micromodel type may be due to initial oil distribution differences in the pore pattern. For MT2 experiments, as for the case of MT1, we observe intersections of at least two confidence intervals for $N_{ca} \in \left[1 \times 10^{-7}; 1 \times 10^{-4}\right]$. MT1_EXP2 presents a positive derivative for $N_{ca} \in \left[8 \times 10^{-7}; 7 \times 10^{-5}\right]$. Concerning MT3 experiments, intervals of confidence globally intercept for every N_{ca}. Starting from around $N_{ca} \approx 3 \times 10^{-6}$, all the MT3 experiments show a period of increase in the oil saturation value. Regarding MT4 experiments, we notice the closeness of the experiments values by pairs, from one side, MT4_EXP1 and MT4_EXP4, and from the other side, MT4_EXP2 and MT4_EXP3.

From the description above, one interesting remark is the group of experiments which present an increase in oil saturation at some stage. This counterintuitive result remained confirmed after image segmentation results were checked in search for possible systematic errors. Therefore, we advance three hypotheses which taken singularly or in combination may cause this effect: Errors coming from the combined chain of image acquisition and segmentation (fluctuations in environmental lighting); oil may have re-entered the micromodel from dead volumes in the inlet/outlet microcircuit; image analysis is suffering from a 2D effect, in other words the real 3D-repartition of the fluids is not accounted for and a pore is accounted as oil-filled only because it is spreading on the upper/lower part of the pore wall (this effect would be obviously spotted out only when it brings an increase in oil saturation but could mislead results in the other sense either).

4 Optimization of the Dataset Information

From the precedent part, we observe specific trends (example: the oil saturation bump seen in MT2_EXP1 at $N_{ca} > 1 \times 10^{-4}$) that cannot be strictly explained as they can come from

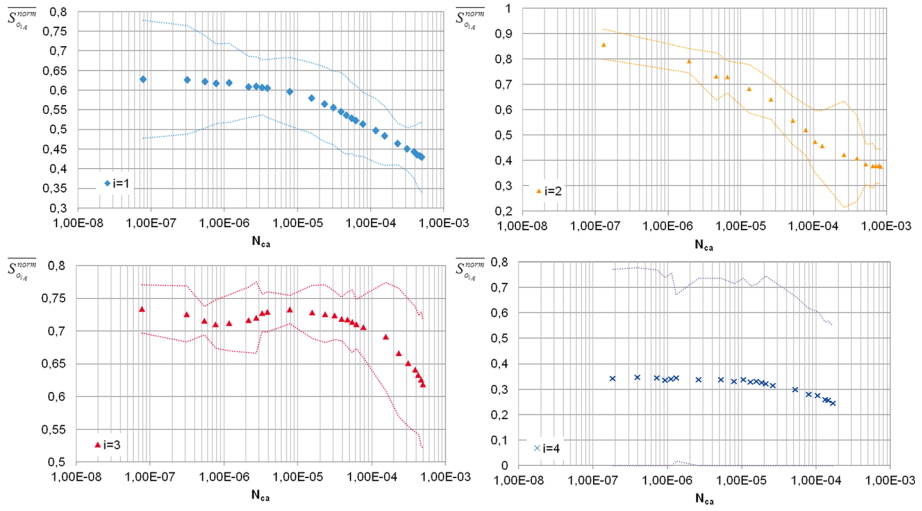

Fig. 7 $\overline{S_{oi,q}^{\text{norm}}}$ in terms of N_{ca} for each micromodel type, the *broken lines* define the uncertainty interval (see Relation 1) associated with the experimental data of the *same color*. For MT4 ($i = 4$), the lowest bound of the uncertainty interval (originally negative) is set to 0

uncontrolled phenomena and which are indistinguishable on a single occurrence basis. Then, in order to averaging the impact of these phenomena, we can perform a statistical analysis for establishing the population estimate $\overline{S_{oi,q}^{\text{norm}}}$ of the oil saturation variable. Note that in this exercise, we do not take into account the historical dependency between experimental states, i.e., we do not consider the correlation between the states at different flow rate (this would require a study on its own).

Note that at this point, we choose $c = 0.95$ as usually considered (Ziliak et al. 2009). With Eqs. 3, 8 and relation 1 (Larson and Farber 2012), we obtain Fig. 7.

$$s_{i,q} = \sqrt{\frac{\sum_{j=0}^{n}(S_{oi,j,q}^{\text{norm}} - \overline{S_{oi,q}^{\text{norm}}})^2}{n-1}} \tag{8}$$

$$\overline{S_{oi,q}^{\text{norm}}} - \frac{t_{n-1}^{c}}{\sqrt{n}} \times s_{i,q} < S_{oi,q}^{\text{norm}} < \overline{S_{oi,q}^{\text{norm}}} + \frac{t_{n-1}^{c}}{\sqrt{n}} \times s_{i,q} \qquad \text{Relation 1}$$

To calculate the combined uncertainty associated with $(\overline{S_{oi,q}^{\text{norm}}})$, $u_c(\overline{S_{oi,q}^{\text{norm}}})$, the b-type uncertainty is considered to be included in the a-type uncertainty (JCGM 2008) as the variability on the measurement of $S_{oi,j,q}^{\text{norm}}$ contributes to the variability of $\overline{S_{oi,q}^{\text{norm}}}$. Then, we have $u_c^2(\overline{S_{oi,q}^{\text{norm}}}) = s_{i,q}^2$. For MT4 data, we obtain a lowest limit of the confidence interval which is negative: For these cases, we choose to set this lowest limit at zero.

In order to quantify the magnitude of the uncertainty interval into the population estimate value, we use Eq. 9 from which we obtain Fig. 8. This figure is an indication of the internal dispersion of the experimental system, in other words the dispersion of the considered phenomenon. One indication of this dispersion is the standard deviation. Nevertheless, as we work with small samples (at most, we have four repetitions of an experiment), this standard deviation is itself distorted by sampling effect: That is why, we multiply the standard deviation by the coefficient $\frac{t_{n-1}^{c}}{\sqrt{n}}$ which incorporates a correction that accounts for the small

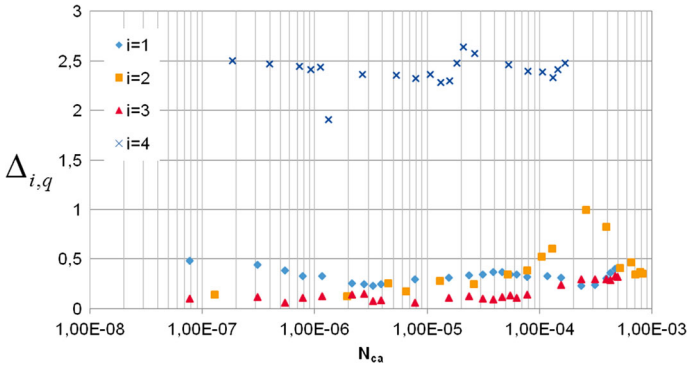

Fig. 8 $\Delta_{i,q}$ (the magnitude of the width interval into the population estimate value) in terms of N_{ca} for each micromodel type (see Eq. 9)

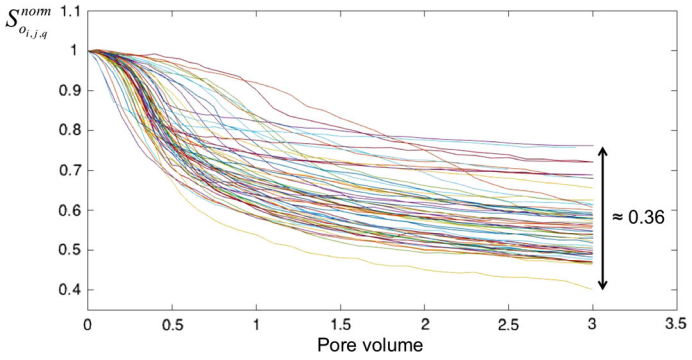

Fig. 9 *Dataset*2 (note that oil saturation can be higher than one due to measurement uncertainty)

sample effect from a general statistical point of view. If we take $\Delta_{i=4,q}$ values, we intuitively see that we can draw poor reliable conclusions from these MT4 data as $\Delta_{i=4,q} > 1$, meaning that the uncertainty on $\overline{S^{\text{norm}}_{o_{i=4,q}}}$ is more than 100%.

$$\Delta_{i,q} = \frac{2 \times \frac{t^c_{n-1}}{\sqrt{n}} \times s_{i,q}}{\overline{S^{\text{norm}}_{o_{i,q}}}} \tag{9}$$

5 Statistical Considerations on Dataset 2

We consider here a micromodel laboratory dataset from our internal historical database (called dataset 2 as described in Material and methods part, paragraph 2). Dataset 2 (Fig. 9) is composed of oil saturation curves in terms of injected pore volume at a fixed capillary number $N_{ca} \approx 4 \times 10^{-8}$ and refers to a different and smaller pore pattern than dataset 1 (see Tables 1, 2). Thus, the objective of studying dataset 2 is to explore the level of microfluidic data dispersion from a statistical point of view, one main interest being the large number of replications as we dispose of 58 replications of a waterflood step (to be compared with the 3 replications we have for the dataset 1). Note that each of these replications starts from the same initial oil saturation ($S^{\text{norm}}_{o_{i,q}} \approx 100\%$ with $i = 5$ and $q = 0$), consequence of performing

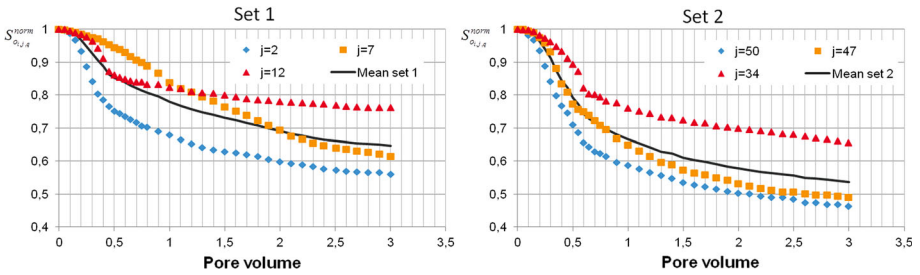

Fig. 10 Oil saturation in terms of pore volume (comparison of two sets of three experiments randomly selected from a database of 58 experiments)

the drainage with extra-heavy oil at $N_{ca} \approx 5 \times 10^{-3}$. Image acquisition frequency is kept coherent in all experiments, one image every 10s approximately: But due to this interval not being exactly regular, we estimated the standard deviation in terms of uncertainty in injected pore volume correspondent to a given image to be 0.06 at most (maximum of the standard deviation of PV calculated for three sets of three randomly taken experiments among dataset 2). Being this interval small, in each of the following plots, the oil saturation data are plotted with the abscissa of the first experiment of that set (always represented by blue diamonds markers). If not specified in text, the values of i and of k are, respectively, 5 and 0.20 μL/h.

5.1 Verification of Small Sampling Effect

In Fig. 10, we present two sets of three experiments, randomly taken among the dataset 2 using the Excel random function. Only three replications by set were selected in order to approach the dataset 1 situation in terms of sampling situation. Note that uncertainty is not shown in this figure as the objective is here to draw qualitative conclusions.

First, we consider the experiments individually. For Set 1, we observe no general trend among the curves. The one labeled $j = 7$ presents a linear behavior (with a determination coefficient of $R^2 \approx 0.98$), whereas $j = 12$ shows an inflexion point at $PV \approx 0.5$ (PV for pore volume). Finally, $j = 2$ has logarithmic shape mainly with $R^2 \approx 0.98$. Regarding, the end oil saturation, there is no evident relation between the three experiments, as this goes from around 25% to nearly 45% (the initial saturation being identical). Note also that the curves $j = 12$ and $j = 7$ intersect at $PV \approx 1$, which is an additional indicator in favor of non-linear offset between the curves. As far as Set 2 is concerned, the curves $j = 50$ and $j = 47$ have a logarithm shape with $R^2 \approx 0.96$ and $j = 34$ presents an inflexion point at $PV \approx 0.6$. Obviously, it is not possible to generalize this behavior into some specific recovery dynamics or trend for this particular crude oil/water/pore system as the variation in curve shape and in the value of final oil saturation is important.

5.2 Reliability and Number of Experiments

One approach to reduce the width of the confidence interval is to increase the size of the dataset considered, noted n. As we dispose of a large initial dataset, we can evaluate the effect of this approach with increasing n and test the inclusion of the total mean (calculated with the 58 values) in the confidence interval. In order to do so, we define the four datasets described in Table 4 represented in Fig. 11. The high limit of the confidence interval is set to 1

Table 4 Description of the considered sets and their statistical enlargement (Chesneau 2015)

Set	a	b	c	d
n	3	7	18	58
t^c_{n-1}	4.303	2.447	2.110	1.836
$\frac{t^c_{n-1}}{\sqrt{n}}$	2.484	0.925	0.497	0.223

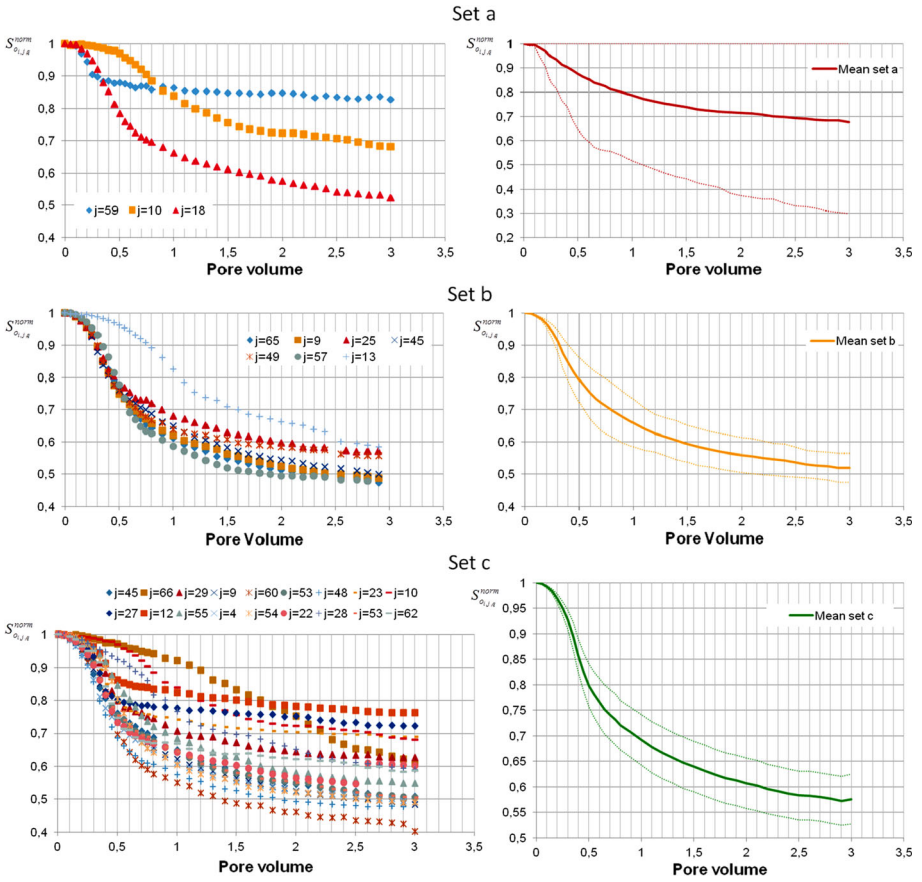

Fig. 11 Graphs on the left represent $S^{\text{norm}}_{o_{i,j,q}}$ in terms of PV for individual experiments that compose the respective dataset; Graphs on the right show the averaged $S^{\text{norm}}_{o_{i,j,q}}$ in terms of PV with the confidence interval in *dashed line*, respectively, for each dataset

if superior to 1. Note that all the sets are composed of randomly chosen individual experiments from the dataset 2; the individual experiments for Set d are not represented as it would not be a relevant illustration due to graph resolution, although the mean is reported in Fig. 12. The composition of Set a was chosen to represent the degree of sampling of the study performed on the dataset 1 and the Set d to consider the larger possible set. Finally, the sampling size of Sets c and d have been, respectively, determined to have a neutral statistical enlargement

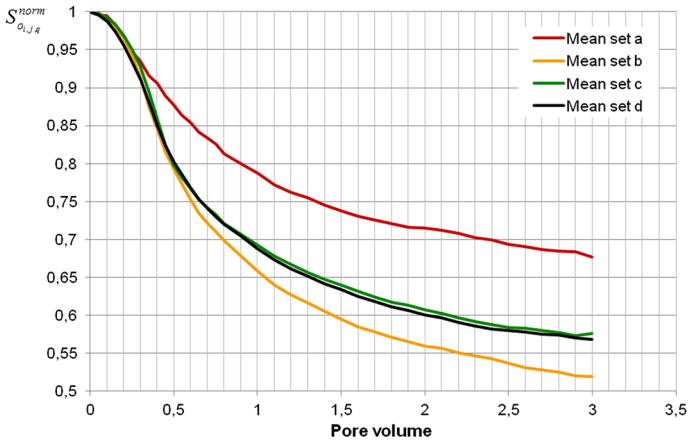

Fig. 12 Comparison of the means of each set in terms of PV

$\left(\frac{t^c_{n-1}}{\sqrt{n}} \approx 1\right)$ and to halve the effect of the sample standard deviation on the confidence interval $\left(\frac{t^c_{n-1}}{\sqrt{n}} \approx 0.5\right)$.

In Fig. 12, we observe that the curves tend to converge to a common value as n increases. Since we can consider that the curve associated with the Set d is the best approximation of the population value as it is the largest set (Larson and Farber 2012), then, if we had to draw quantitative conclusions on final recovery from Set a only, these would be far off by around 10% saturation units, which can be considered a poor outcome. On top of this, we must also consider that the fluctuations for sets of three experiments are significant: With this sampling rate and with such a natural dispersion in waterflooding data, it is questionable whether quantitative information could be derived for the successive desaturation experiment, were this to be performed.

This effect is now shown in Fig. 13 where MATLAB® software was used to perform random draws (without replacement, with the function *randsample*) of $m = 10$ realizations of sets of $n = 3$, 7 and 18 experiments, respectively. To characterize the variability as n increases, we extend and rearrange the data in Fig. 14 in terms of $\Delta_{m,n}$ corresponding to Eq. 10.

$$\Delta_{m,n} = \frac{2 \times \frac{t^c_{n-1}}{\sqrt{n}} \times s_{m,n}}{\overline{S^{\text{norm}}_{o_{m,n}}}} \tag{10}$$

where $s_{m,n}$ is the standard deviation of the mean curves at $PV \approx 3$, and $\overline{S^{\text{norm}}_{o_{m,n}}}$ is the oil saturation mean of the $m = 10$ realizations (the red circles in Fig. 13) taken at $PV \approx 3$.

In conclusion, for the system under study and for these randomly selected sets, a set of three experiments is a poor qualitative indicator of a specific variable such as oil recovery: We see from our example that increasing the number of replications to at least 7 begins to provide much closer approximations of the true value by averaging. In the limit of this sampling work, we can estimate that with $n \leq 7$ only general qualitative information can be drawn such as the increase in oil saturation with the injected pore volume. For $n \geq 7$, however, it is possible to draw quantitative information, such as the speed of the oil saturation decrease (derivative of the curve), according to the precision wanted. Note that we define qualitative information as any statement on the data that is non-numerical in nature, whereas

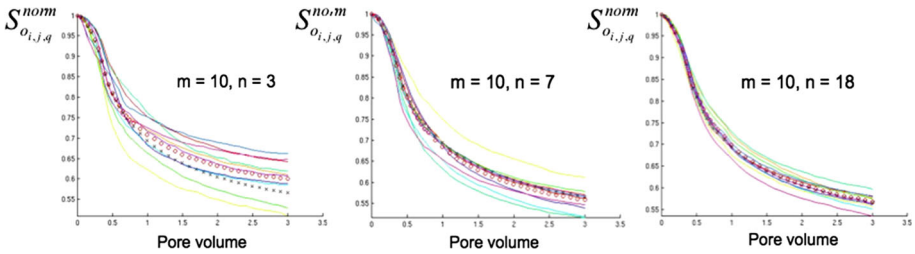

Fig. 13 Averaged oil saturation $S^{\text{norm}}_{o_{i,j,q}}$ in terms of pore volume for m sets of n experiments randomly drawn; each colored curve represents the mean of an "n-experiments" set, the *red circles* represent the mean of these curves and the *black crosses* are the mean on all the experiments from dataset 2

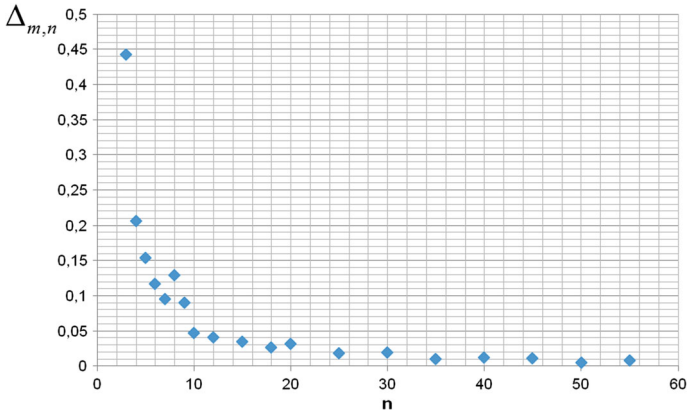

Fig. 14 $\Delta_{m,n}$ in terms of n; normalization is made with the mean on the 10 set's means (*red circles* on Fig. 13) taken at $PV \approx 3$

quantitative information is anything that uses numbers for examining the relationship among variables (Creswell 2014).

In general, the number of experiments n that is to be performed must be defined according to the degree of variability allowed for the wanted information. One may use the tool Δ to present and define this variability as a value and also define acceptability standards for the repeatability of the experiment.

6 Conclusion

A comprehensive study has been performed on two micromodel datasets with the aim to present their variability in terms of CDC and waterflood results. The objective is to verify the statistical representativeness of data provided by micromodels in light of possible utilizations as a screening tool for qualifying performance of oil recovery protocols. The first point has been the observation, conducted also on an external dataset, that these types of experiments can be subject to an important degree of data dispersion; then, as expected by statistics, a greater number of replications is associated with greater trueness. One approach is to categorize the data according to the magnitude of the dispersion on the average value (for a fixed experimental step and a given data variable), and for this, we have considered the parameter Δ and the two following categories: qualitative and quantitative. Thus, the number

of experiments n has to be settled in order to define these categories. n can be chosen by the experimental team on pragmatic bases (costs, time, human resources…) but also by considering the internal dispersion of the studied physical system. In particular, with the dataset 2, we have exposed an application of these precedent guidelines and determined that quantitative information on non-wetting phase recovery, with the consideration of a confidence interval, can be drawn for $n \geq 7$. This is to minimize the statistical enlargement (i.e., when $\frac{t^c_{n-1}}{\sqrt{n}} \geq 1$) in order to approach the true value. Finally, to test the robustness of this statement, the parameter Δ has been applied to the mean of datasets and the obtained results show a significant monotonic trend that strengthens the possibility to determine a threshold on n. This work demonstrated the challenge of drawing robust quantitative oil recovery conclusions from micromodel datasets without statistical work: It is either an approach to optimize the utilization of the data or a method to prevent flawed notions. A general obvious statement from this work is that to draw quantitative and even certain type of qualitative information on recovery performance from micromodel experiments requires more than a single experiment (which is generally not the case in the investigated literature). We hope that our work will convince of the need of more systematic experiment repeatability verification for micromodel experiments in the field of fluid mechanics as well as in any that includes data from micromodels. Repeatability verification is also key in helping to determine any experimental reason leading to data dispersion and then operate to reduce its impact.

Acknowledgements The authors are grateful to TOTAL S.A. for the financial and technical contribution and to Jean-Philippe Chaulet for his technical assistance during this study. The personnel at the Geoscience Research Centre of TOTAL UK in Aberdeen, Scotland, is also gratefully acknowledged.

References

AlDousary, S.: Determining pore level mechanisms of alkaline surfactant polymer flooding using a micromodel. Soc. Petrol. Eng., 165572-STU (2012)

Alireza, E., Sohrabi, M.: Visula investigation of oil recovery by low salinity water injection: formation of water micro-dispersions and wettability alteration. Soc. Petrol. Eng. 166435 (2013)

Armstrong, R.T., Berg, S.: Interfacial velocities and capillary pressure gradients during Haines jumps. Phys. Rev. **88**, 043010 (2013)

Armstrong, R.T., Evseev, N., Koroteev, D., Berg, S.: Modeling the velocity field during Haines jumps in porous media. Adv. Water Resour. **77**, 57–68 (2015)

BIPM: Evaluation of measurement data—guide to the expression of uncertainty in measurement (GUM 1995 with minor corrections), vol. 100. JCGM, Montrouge (2008)

Bondino, I., Doorwar, S., Ellouz, R., Hamon, G.: Visual microscopic investigations about the role of ph, salinity and clay on oil adhesion and recovery. International Symposium of the Society of Core Analysts held in Napa Valley, California (2013)

Buchgraber, M., Al-Dossary, M., Ross, C.M., Kovscek, A.R.: Creation of a dual-porosity micromodel for pore-level visualization of multiphase flow. J. Petrol. Sci. Eng. **86–87**, 27–38 (2012)

Buchgraber, M., Clemens, T., Castanier, L.M., Kovscek, A.R.: A microvisual study of the displacement of viscous oil by polymer solutions. Soc. Petrol. Eng. 122400 (2011). doi:10.1016/j.petrol.2012.03.012

Chatzis, I., Morrow, N.R.: Correlation of capillary number relationship for sandstone. Soc. Petrol. Eng. (1984). doi:10.2118/10114-PA

Chatzis, I., Morrow, N., Lim, H.: Magnitude and detailed structure of residual oil saturation. Soc. Petrol. Eng. J. (1983). doi:10.2118/10681-PA

Chesneau, C.: Tables de valeurs. Retrieved 2015 3-November from Université , de Caen Basse-Normandie. http://www.math.unicaen.fr/~chesneau/tables-valeurs.pdf (2015)

Cottin, C., Bodiguel, H., Colin, A.: Drainage in two-dimensional porous media: from capillary fingering to viscous flow. Phys. Rev. **82**, 046315 (2010)

Cottin, C., Bodiguel, H., Colin, A.: Influence of wetting conditions on drainage in porous media: a microfluidic study. Phys. Rev. **84**, 026311 (2011)

Creswell, J.W.: Research Esign: Qualitative, Quantitative and Mixed Methods Approaches, 4th edn. SAGE Publication, Beverley Hills (2014)
Datta, S.S., Dupin, J.-B., Weitz, D.A.: Fluid breakup during simultaneous two-phase flow through a three-dimensional porous medium. AIP Publ. **26**, 062004 (2014)
Datta, S.S., Ramakrishnan, T.S., Weitz, D.A.: Mobilization of a trapped non-wetting fluid from a three-dimensional porous medium. AIP Publ. **26**, 022002 (2014)
Doorwar, S., Mohanty, K.K.: Extension of the dielectric breakdown model for simulation of viscous fingering at finite viscosity ratios. Phys. Rev. **90**, 013028 (2014)
Emadi, A., Sohrabi, M.: Visual investigation of low salinity waterflooding. International Symposium of the Society of Core Analysts held in Aberdeen, Scotland (2012)
Iglauer, S., Ferno, M., Shearing, P., Blunt, M.: Comparison of residual oil cluster size distribution, morphology and saturation in oil-wet and water-wet sandstone. Elsevier, London. doi:10.1016/j.jcis.2012.02.025 (2012)
Jadhunandan, P., Morrow, N.: Effect of wettability on waterflood recovery for crude-oil/brine/rock systems. SPE Reserv. Eng. (1995). doi:10.2118/22597-PA
Karadimitriou, N.K., Hassanizadeh, S.M.: A review of micrmodels and their use in two-phase flow studies. Soil Sci. Soc. Am. 0021-0041 (2011)
Karadimitriou, N., Hassanizadeh, S.: A review of micromodels and their use in two-phase flow studies. Soil Sci. Soc. Am. doi:10.2136/vzj2011.0072 (2012)
Larson, R., Farber, B.: Elementary Statistics: Picturing the World, 5th edn. Pearson Education Inc, Boston (2012)
Levaché, B.: Dynamique d'imbibition en milieu confiné (Ph.D. thesis). Paris: Université Pierre et Marie Curie (UPMC) (2014)
Porter, M.L., Jiménez-Martinez, J., Carey, J.W., Viswanathan, H., Mody, F., Sheng, J.: Fundamental investigation of gas injection in microfluidic shale fracture networks at geologic conditions. Am. Rock Mech. Assoc. 15-0367 (2015). https://www.onepetro.org/conference-paper/ARMA-2015-367
Rodriguez de Castro, A., Shokri, N., Karadimitriou, N., Oostrom, M., Joekar-Niasar, V.: Experimental study on nonmonotonicity of capillary desaturation curves in a 2-D pore network. Water Resour. Res. **51**, 8517–8528 (2015)
Schneider, M.: Wettability patterning in microfluidic systems and applications on the petroleum industry. Ph.D. of Pierre and Marie Curie University (2011)
Sedaghat, M.H., Ghazanfari, M.H., Parvazdavani, M., Morshedi, S.: Experimental investigation of microscopic/macroscopic effeciency of polymer flooding in fractured heavy oil five-spot systems. J. Energy Resour. Technol. **135**, 032901-1 (2013)
Sohrabi, M., Emadi, A., Farzaneh, S. A., and Ireland, S.: A thorough investigation of mechanisms of enhanced oil recovery by carbonated water injection. Soc. Petrol. Eng. 175159-MS (2015)
Song, W., Kovscek, A.R.: Functionalization of micrmodels with kaolinite for investigation of low salinity oil-recovery processes. R. Soc. Chem. **15**, 3314 (2015)
Taylor, J.R.: Incertitudes et analyse des erreurs dans les mesures physiques—Avec exercices corrigés. DUNOD—Collection Masson Sciences (2000)